

International Journal of Modern Physics E
 © World Scientific Publishing Company

Effects of transient non-thermal particles on the big bang nucleosynthesis

Tae-Sun Park^{†,††}, Kyung Joo Min[‡] and Seung-Woo Hong^{†,‡,*}

[†]*Department of Physics, Sungkyunkwan University
 Suwon 16419, Korea*

^{††}*Center for Exotic Nuclei Studies, Institute for Basic Science
 Daejeon 34126, Korea*

[‡]*Department of Energy Science, Sungkyunkwan University
 Suwon 16419, Korea
 swhong@skku.ac.kr

Received Day Month Year
 Revised Day Month Year

The effects of introducing a small amount of non-thermal distribution (NTD) of elements in big bang nucleosynthesis (BBN) are studied by allowing a fraction of the NTD to be time-dependent so that it contributes only during a certain period of the BBN evolution. The fraction is modeled as a Gaussian-shaped function of $\log(T)$, where T is the temperature of the cosmos, and thus the function is specified by three parameters; the central temporal position, the width and the magnitude. The change in the average nuclear reaction rates due to the presence of the NTD is assumed to be proportional to the Maxwellian reaction rates but with temperature $T_{\text{NTD}} \equiv \zeta T$, ζ being another parameter of our model. By scanning a wide four-dimensional parametric space at about half a million points, we have found about 130 points with $\chi^2 < 1$, at which the predicted primordial abundances of light elements are consistent with the observations. The magnitude parameter ε_0 of these points turns out to be scattered over a very wide range from $\varepsilon_0 \sim 10^{-19}$ to $\sim 10^{-1}$, and the ζ -parameter is found to be strongly correlated with the magnitude parameter ε_0 . The temperature region with $0.3 \times 10^9 \text{K} \lesssim T \lesssim 0.4 \times 10^9 \text{K}$ or the temporal region $t \simeq 10^3$ s seems to play a central role in lowering χ^2 .

Keywords: Big bang nucleosynthesis; transient; non-thermal distribution

PACS numbers: 26.35.+c, 26.40.+r, 98.80.Ft

1. Introduction

Big bang nucleosynthesis (BBN) serves as the standard scenario to address the primordial abundances of light elements of our universe.^{1–6} With the baryon-to-photon ratio η_0 determined accurately by the cosmic microwave background radiation measurement of Wilkinson Microwave Anisotropy Probe⁷ and Planck,⁸ BBN is basically parameter-free and can explain the abundances of primordial deuteron

*Corresponding author

2 *Authors' Names*

and ${}^4\text{He}$ quite successfully. However, the BBN prediction for lithium is reported to be about three times bigger than the observation,^{9–13} and has brought a lot of attention (see Refs. 14, 15, for instance).

Incidentally, a puzzling drop in Li/H in metal-poor stars has been observed,¹⁶ which imposes a substantial uncertainty on the primordial Li abundance. We refer to, for example, Refs. 17–20 for stellar models that take into account detailed mechanisms of the Li depletion in those stars. These models, however, do not resolve the Li discrepancy completely.²¹

There have been theoretical efforts to resolve the above so-called “lithium problem” by altering the assumption that all particles except neutrinos are at thermal equilibrium with the Maxwellian distribution. For example, the in-flight reaction probability has been extensively studied^{22, 23} by taking into account the fact that the particles created from nuclear reactions can have energies in the MeV range and thus can have a probability of overcoming the Coulomb repulsion to go through nuclear reactions before being thermalized. The effect of such a mechanism turns out to be insufficient to change the abundance significantly. Another interesting approach was attempted by Bertulani et al.,²⁴ where the Maxwell-Boltzmann (MB) distribution was modified to adopt the so-called non-extensive statistics with the results that it only worsens the lithium problem.

Our study is closely related to the work by Kang et al.,²⁵ where they have introduced so-called “cosmic rays”, which consist of only proton isotopes (protons, deuterons and tritons) that are assumed to have a power-law shaped distribution up to 4 MeV. In the study of Kang et al.,²⁵ the upper limit of the distribution is severely constrained since cosmic rays with energies higher than the $D(p, n)\text{H}_2$ threshold, 3.337 MeV, destroy deuterium. By tuning the fraction of the cosmic rays with respect to thermal isotopes of hydrogen to 0.7×10^{-6} , they could account for the lithium abundance successfully, but with a 5 % reduction of the deuteron abundance. In their approach, the fraction of particles (denoted by ε) with non-Maxwellian distribution was treated as time-independent. This assumption may be questioned in that the cosmic rays with such a non-MB distribution may exist only for a certain period rather than being independent of time or temperature.

The question on the origin of the time-dependent cosmic rays is not addressed here, but there are candidates related to, but not limited to, decay or annihilation of relic particles, which would inject cosmic rays to the universe. The outgoing particles of decay processes of relic particles would be rapidly thermalized due to the interactions with background materials, but the decay or annihilation rate will have a non-trivial time-dependence characterized by the lifetimes or the time-dependence of the energies and densities of the relic particles. For example, the decay of the next lightest supersymmetric particle (NLSP) into the lightest supersymmetric particle (LSP) dark matter can produce time-dependent suprathreshold particles. Indeed, it was discussed that the stau-NLSP and gravitino-LSP system with stau lifetime $\tau \simeq 10^3$ s could resolve the lithium problem with some representative values of the

model parameters.²⁶ We refer to Ref. 27 and references therein for a comprehensive review on the role of dark matter on the BBN.

In this work, we do not stick to any particular scenario or candidate for the origin of cosmic rays. Instead, we explore the possibility in which the fraction of the NTD is a function of time or temperature. Since temperature is a monotonically decreasing function of time, time dependence can be converted to temperature dependence. The time dependence of the fraction $\varepsilon(T)$ is modeled as a Gaussian-shaped function of $\log(T)$ with three parameters for the central temporal position T_0 , the width Δ , and the magnitude ε_0 : An explicit functional form will be given in the next section. Although a power-law type distribution would be a reasonable approach, making a realistic model for the non-MB distribution requires an initial condition and the evolution with time. Thus, we make a naive assumption for computational convenience by assuming that the averaged reaction rate $\langle\sigma v\rangle_{ij\rightarrow kl}(T)$ in the presence of the NTD can be approximated as a sum of two Maxwellian reaction rates of particles at temperatures T and T_{NTD} , *i.e.*,

$$\langle\sigma v\rangle_{ij\rightarrow kl}(T) = [1 - \varepsilon(T)] R_{ij\rightarrow kl}^{th}(T) + \varepsilon(T) R_{ij\rightarrow kl}^{th}(T_{\text{NTD}}), \quad (1)$$

where the subscript “ $ij \rightarrow kl$ ” is the reaction index, T_{NTD} stands for “the temperature of the NTD”, and $R_{ij\rightarrow kl}^{th}(T)$ is the usual Maxwell-Boltzmann averaged reaction rate in thermal equilibrium at temperature T . We introduce $\zeta \equiv T_{\text{NTD}}/T$ and treat ζ as a free parameter. Since the non-thermal particles with temperatures less than T would not change the reaction rates significantly, the parameter ζ is expected to be larger than unity. This assumption of a Maxwell-Boltzmann reaction rate for the NTD simplifies the calculation significantly.

We then scan a wide range of four-dimensional parameter space of $(\varepsilon_0, T_0, \Delta, \zeta)$, searching for the best parameters that meet the observational data for the primordial abundances. The details of our model and the calculational method are described in Sec. II, which is followed by the results in Sec. III, and discussions in Sec. IV.

2. Calculational method

Let us begin with the discussion of the assumption in Eq. (1). The averaged reaction rate of the reaction $i + j \rightarrow k + l$ reads

$$\langle\sigma v\rangle_{ij\rightarrow kl}(T) = \frac{1}{2} \int_{-1}^1 d \cos \theta_{ij} \int_0^\infty dE_i \int_0^\infty dE_j v_{ij} \sigma_{ij\rightarrow kl} f_i(E_i, T) f_j(E_j, T), \quad (2)$$

where θ_{ij} is the relative angle, v_{ij} is the relative velocity, $\sigma_{ij\rightarrow kl}$ is the cross section of the reaction, and $f_i(E_i, T)$ is the distribution of the i -th particle with energy E_i . Equation (2) can be rewritten as an integration over the center-of-mass energy E_{ij} ,

$$\langle\sigma v\rangle_{ij\rightarrow kl}(T) = \int_0^\infty dE_{ij} v_{ij} \sigma_{ij\rightarrow kl} F_{ij}(E_{ij}, T). \quad (3)$$

4 Authors' Names

When all the incoming particles are in thermal equilibrium with Maxwellian distribution, $f_i(E_i, T) = f^{th}(E_i, T) \equiv 2\sqrt{E_i/\pi(kT)^3}e^{-E_i/kT}$, $F_{ij}(E_{ij}, T)$ becomes identical to the Maxwell-Boltzmann distribution, $F_{ij}(E_{ij}, T) = f^{th}(E_{ij}, T)$. In the presence of non-thermal components, the i -th particle's distribution can be written as

$$f_i(E_i, T) = [1 - \varepsilon_i(T)] f^{th}(E_i, T) + \varepsilon_i(T) f_i^{ntd}(E_i, T) \quad (4)$$

with the normalization condition $\int_0^\infty dE_i f_i^{ntd}(E_i, T) = 1$, where $f_i^{ntd}(E_i, T)$ is a yet unknown distribution of the non-thermal part, and $\varepsilon_i(T)$ is its temperature-dependent magnitude. Then F_{ij} reads in non-relativistic limit

$$F_{ij}(E_{ij}, T) = (1 - \varepsilon_i)(1 - \varepsilon_j) f^{th}(E_{ij}, T) + \int_0^\infty dE_i \int_{E_{j-}}^{E_{j+}} dE_j \frac{\mathcal{F}_{ij}^{ntd}}{2\mu v_i v_j} \quad (5)$$

with

$$\begin{aligned} \mathcal{F}_{ij}^{ntd} &= \varepsilon_i(1 - \varepsilon_j) f_i^{ntd}(E_i, T) f^{th}(E_j, T) \\ &+ (1 - \varepsilon_i)\varepsilon_j f^{th}(E_i, T) f_j^{ntd}(E_j, T) \\ &+ \varepsilon_i \varepsilon_j f_i^{ntd}(E_i, T) f_j^{ntd}(E_j, T), \end{aligned} \quad (6)$$

where $\varepsilon_i = \varepsilon_i(T)$, $\mu = m_i m_j / (m_i + m_j)$, $v_{ij} = \sqrt{2E_{ij}/\mu}$, $v_i = \sqrt{2E_i/m_i}$, and $E_{j\pm} = \frac{1}{2}m_j(v_{ij} \pm v_i)^2$. Instead of modeling f_i^{ntd} , we assume that $F_{ij}(E_{ij}, T)$ may be effectively approximated as

$$F_{ij}(E_{ij}, T) = [1 - \varepsilon(T)] f^{th}(E_{ij}, T) + \varepsilon(T) f^{th}(E_{ij}, T_{NTD}), \quad (7)$$

where $\varepsilon(T)$ is the amount of the NTD to be taken as T -dependent and is to be discussed shortly. Combining Eqs.(3) and (7), and defining $R_{ij \rightarrow kl}^{th}(T)$ by

$$R_{ij \rightarrow kl}^{th}(T) \equiv \int_0^\infty dE_{ij} v_{ij} \sigma_{ij \rightarrow kl} f^{th}(E_{ij}, T), \quad (8)$$

we are led to Eq. (1). One of the immediate advantages in this approach is that we can make use of the well-established codes²⁸⁻³⁶ available for the standard BBN calculations without having to write extra codes for the averaged reaction rates in the presence of NTD particles.

Before going further, let us remark on the reverse rates. In the presence of NTD, our assumption given in Eq. (1) implies the inverse rate $kl \rightarrow ij$ to be

$$\langle \sigma v \rangle_{kl \rightarrow ij}(T) = [1 - \varepsilon(T)] R_{kl \rightarrow ij}^{th}(T) + \varepsilon(T) R_{kl \rightarrow ij}^{th}(T_{NTD}). \quad (9)$$

As is the case with $R_{kl \rightarrow ij}^{th}(T)$, the reverse rate $R_{kl \rightarrow ij}^{th}(T_{NTD})$ is computed from $R_{ij \rightarrow kl}^{th}(T_{NTD})$ by using the time reversal symmetry with the assumption of thermal equilibrium at temperature T_{NTD} . Because both $R_{ij \rightarrow kl}^{th}(T)$ and $R_{ij \rightarrow kl}^{th}(T_{NTD})$ satisfy the principle of the detailed balance, the total reverse rate also does.

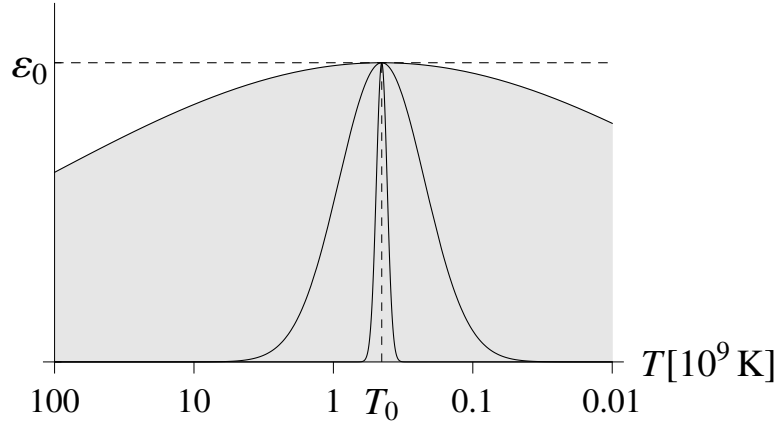


Fig. 1: The NTD portion $\varepsilon(T)$ for $T_0 = 0.45 \times 10^9 \text{K}$, and $\Delta = 4$ (outermost), 1 (middle) and 0.0625 (innermost).

In the consideration of the time or temperature dependence of the amount of NTD portion, the dependence of $\varepsilon(T)$ on T is taken as a Gaussian-shaped function peaked at T_0 with a "window" of width Δ and peak height ε_0 ,

$$\varepsilon(T) = \varepsilon_0 \exp \left[- \left(\frac{\log(T/T_0)}{\Delta} \right)^2 \right]. \quad (10)$$

Note that $\varepsilon(T)/\varepsilon_0 \geq 1/e$ only in the region $T_0 e^{-\Delta} \leq T \leq T_0 e^{\Delta}$. To illustrate the dependence of $\varepsilon(T)$ on Δ , which corresponds to the length of time during which NTD particles appear, we show $\varepsilon(T)$ for $T_0 = 0.45 \times 10^9 \text{K}$ and three values of Δ in Fig. 1. Since the NTD portion is concentrated around $T \simeq T_0$, $T_{\text{NTD}} = \zeta T$ may be regarded as $T_{\text{NTD}} \simeq \zeta T_0$, especially when the width parameter Δ is small.

Here we would like to mention that our choice for the shape of the fraction $\varepsilon(T)$ as a Gaussian is a naive ansatz chosen for computational convenience. An exponentially decaying shape, for example, could be a more suitable choice for many scenarios of the NTD. However, since we will scan the parametric space with varying the width of $\varepsilon(T)$, the major effect due to the presence of the NTD particle may be captured regardless of the details of the functional form.

Let us now describe how the parameter space is scanned. For the magnitude parameter ε_0 , we scan quite a large range by choosing $n = 1$ to 30 in $\varepsilon_0 = 10^{-n}$ to see the possibility that even a very tiny fraction of NTD may affect the lithium problem. Most important nuclear synthesis occurs around $T \sim (0.1 \sim 1) \times 10^9 \text{K}$, and thus for the peak temperature parameter T_0 we choose 41 grid points in the $\log(T_0)$ axis from $T_{09} \equiv T_0/10^9 \text{K} = 0.1$ to 1 by setting $T_{09} = 10^{n/40}$ with $n = -40$ to 0. The width parameter Δ is chosen to vary from 0.0625 to 4 by doubling the values

6 *Authors' Names*

Table 1: Particle Data Group data and the SBBN prediction for the primordial abundances.

	D/H [10^{-5}]	Y_p	Li/H [10^{-10}]	Reference
PDG (2012)	2.82 ± 0.21	0.249 ± 0.009	$1.7 \pm 0.06 \pm 0.44$	37
PDG (2014)	2.53 ± 0.04	0.2465 ± 0.0097	1.6 ± 0.3	38
SBBN	2.49 ± 0.17	0.2486 ± 0.0002	$5.24^{+0.71}_{-0.62}$	39

of Δ , that is, $\Delta = 2^n$ with $n = -4$ to 2. As shown in Fig. 1, $\Delta = 0.0625$ is narrow enough to explore the possibility of locating the period of time for non-thermal disturbance which can affect the BBN results, and $\Delta = 4$ is big enough for $\varepsilon(T)$ to be essentially regarded as independent of T . The ratio of the NTD-temperature to the temperature of the cosmos, $\zeta = T_{\text{NTD}}/T$, is chosen to be $\zeta = 10^{n/40}$ with $n \geq 1$. Since the Kawano code is supposed to be accurate only up to $T_9 \equiv T/10^9\text{K} \lesssim 10$ and the reliability of the calculation for $\zeta T_{09} \gtrsim 10$ is highly questionable, we set an upper limit to the ζ parameter by imposing the condition $\zeta T_{09} \leq 10$, i.e., $n \leq 40$ for $T_{09} = 1$ and $n \leq 80$ for $T_{09} = 0.1$. In this search scheme, the total number of grid points considered is $30 \times 41 \times 7 \times (40 + 80)/2 = 516,600$, which can be summarized as follows:

$$\begin{aligned}
\varepsilon_0 &= [10^{-1}, 10^{-2}, 10^{-3}, \dots, 10^{-30}], \\
T_{09} &= [10^{-1}, 10^{-0.975}, 10^{-0.95}, \dots, 10^0], \\
\Delta &= [0.0625, 0.125, 0.25, \dots, 4], \\
\zeta &= [10^{0.025}, 10^{0.05}, 10^{0.075}, \dots, 10/T_{09}].
\end{aligned} \tag{11}$$

At each grid point, we evaluate χ^2 defined by

$$\chi^2 = \left| \chi(\text{D}/\text{H}|_p) \right|^2 + \left| \chi(Y_p) \right|^2 + \left| \chi(\text{Li}/\text{H}|_p) \right|^2 \tag{12}$$

with

$$\chi(\alpha) \equiv \frac{\mathcal{C}(\alpha) - \mathcal{O}(\alpha)}{\sigma(\alpha)}, \tag{13}$$

where $\mathcal{C}(\alpha)$, $\mathcal{O}(\alpha)$ and $\sigma(\alpha)$ stand for the calculated value, the observed value, and the uncertainty for the quantity α , respectively. For $\mathcal{O}(\alpha)$ and $\sigma(\alpha)$, we adopt the PDG(2014) data listed in Table 1.

Here and hereafter, what we mean by Li in Eq. (12) is the sum of ${}^6\text{Li}$, ${}^7\text{Li}$ and ${}^7\text{Be}$. This is because all the primordial ${}^7\text{Be}$ decays to ${}^7\text{Li}$, and what is measured is the sum of ${}^6\text{Li}$ and ${}^7\text{Li}$, not just ${}^7\text{Li}$, though the amount of primordial ${}^6\text{Li}$ is orders of magnitude less than that of ${}^7\text{Li}$.

For the calculation, we adopt the so-called Kawano code.^{28–36}

3. Results

3.1. Distribution of χ^2 in the parameter space

The results of our calculations of χ^2 are presented in the three-dimensional parameter space $(\zeta, \varepsilon_0, T_{09})$ in Fig. 2 for a few selected values of Δ by drawing rectangular boxes whose sizes are proportional to the value of $\exp(-\chi^2/3)$ at each grid site for the cases when the value of $\chi^2 \leq 3$. The projections of the rectangular boxes are also shown on the three planes in the parameter space $(\zeta, \varepsilon_0, T_{09})$.

Figure 2(a) shows that when the width parameter is as small as $\Delta = 0.0625$, the parameter set with a small χ^2 are located in a narrow temperature range with $0.37 \lesssim T_{09} \lesssim 0.43$. This band structure becomes irregular as Δ becomes bigger, and then disappears for $\Delta \geq 1$. We may understand this result as follows. Equation (10) implies that the magnitude of the non-thermal distribution $\varepsilon(T)$ is non-trivial only during the period when the temperature lies in $T \simeq T_0(e^{-\Delta} \sim e^{\Delta})$; otherwise the magnitude is exponentially suppressed. If Δ is small, the NTD is effective only in a narrow range around $T \simeq T_0$, and thus the χ^2 minimum can be localized in the T_0 space. The results with a small Δ in Fig. 2 imply that the NTD contribution in the narrow range around $T \simeq 0.40 \times 10^9\text{K}$ plays the key role in lowering χ^2 . On the other hand, if Δ is large, $\varepsilon(T)$ becomes less sensitive to the T_0 parameter. As long as the “window” of $\varepsilon(T)$ overlaps to some extent with the temperature range around $T \simeq 0.40 \times 10^9\text{K}$, there is a potential to cure the lithium problem. The estimation of the range of T_{09} by using $T_{09} \simeq 0.4 \times (e^{-\Delta} \sim e^{\Delta})$, inferred from Eq. (10) gives us $T_{09} \simeq (0.38 \sim 0.43)$ for $\Delta = 0.0625$, $T_{09} \simeq (0.31 \sim 0.51)$ for $\Delta = 0.25$ and $T_{09} \simeq (0.15 \sim 1)$ for $\Delta = 1$, which are more or less consistent with Fig. 2. Fig. 2(d) shows there are not many grid points where $\chi^2 \leq 3$ when $\Delta = 4$. As will be shown in subsection 3.2, we cannot find good parameter sets with $\chi^2 \leq 3$ if $\Delta = 4$. Thus, the width parameter Δ seems to be limited to $\Delta = 1$ or less.

As can be seen from the projections plotted on the bottom plane in Fig. 2, the parameter $\zeta = T_{\text{NTD}}/T$ turns out to be strongly correlated with ε_0 . This is natural because the amount of the NTD portion required to cure the lithium problem would be smaller if the temperature of the NTD becomes higher. It is noteworthy that the correlation curves are quite insensitive to the value of Δ , which can be seen by comparing the projections in the (ε_0, ζ) plane for different values of Δ in Fig. 2. The projection of $\exp(-\chi^2/3)$ on the (ε_0, ζ) plane is displayed in Fig. 3, where the value of Δ is adjusted to yield the minimum χ^2 at each grid site. If ζ is chosen as 20, 10 and 5, the required fraction to yield a small χ^2 becomes $\varepsilon_0 \simeq 10^{-17}$, 10^{-15} and 10^{-11} , respectively.

In Fig. 4, $\exp(-\chi^2/3)$ is plotted in the (ε_0, T_{09}) plane for a few selected values of Δ . At each grid point, the value of ζ is further adjusted to produce the minimum χ^2 while its rough value can be inferred from the aforementioned correlation curve between ε_0 and ζ . Figure 4 demonstrates, in particular, how the band-type structure observed around $T_{09} \simeq 0.40$ for a small Δ evolves as Δ becomes large. For a width parameter Δ in the medium range, such as $\Delta = 0.25$, the band is formed in the

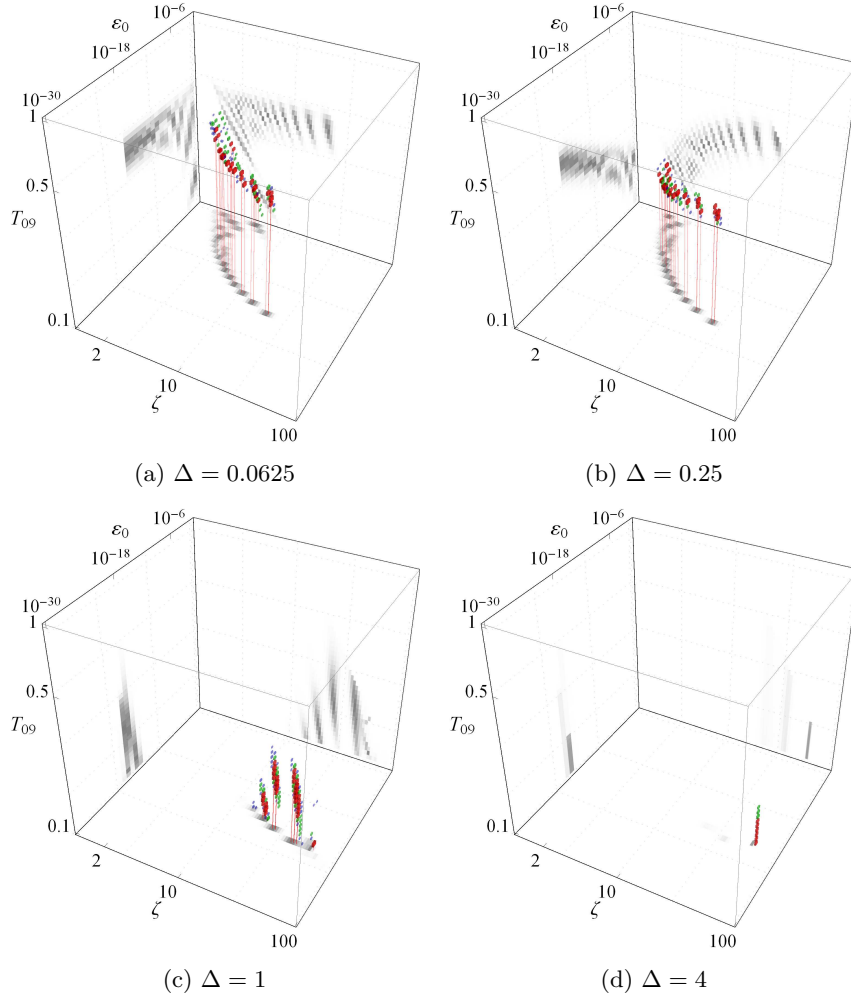
8 *Authors' Names*

Fig. 2: The χ^2 values are plotted in the three-dimensional parameter space $(\varepsilon_0, \zeta, T_{09})$ for $\Delta = 0.0625$ (a), 0.25 (b), 1 (c) and 4 (d). Though the grids are not shown here, the grid points at which $\chi^2 \leq 3$ are represented by rectangular boxes, whose sizes are proportional to the value of $e^{-\chi^2/3}$. The boxes are colored according to the value of χ^2 : Red for $\chi^2 \leq 1$, green for $1 < \chi^2 \leq 2$ and blue for $2 < \chi^2 \leq 3$. For the cases where $\chi^2 \leq 1$, thin lines are drawn to guide the eyes from the boxes down to the bottom plane. The boxes are projected to the three planes (ε_0, ζ) , (ζ, T_0) , and (T_0, ε_0) , where a darker gray color corresponds to a smaller χ^2 .

diagonal direction in the (ε_0, T_{09}) plane, while the band is rotated to the direction of constant $\varepsilon_0 \sim 10^{-18}$ for $\Delta = 1$ or larger.

Table 2: 12 points in the parametric space which have $\chi^2 < 0.1$. To get the values of χ^2 per degree of freedom, 1/3 needs to be multiplied by the values in the Table.

No	χ^2	ε_0	Δ	ζ	T_{09} [10^9K]	D/H [10^{-5}]	T/H [10^{-8}]	$^3\text{He}/\text{H}$ [10^{-5}]	$^6\text{Li}/\text{H}$ [10^{-14}]	$^7\text{Li}/\text{H}$ [10^{-10}]	$^7\text{Be}/\text{H}$ [10^{-10}]
1	0.006	10^{-12}	0.2500	5.62	0.282	2.528	5.692	0.844	1.091	0.242	1.355
2	0.011	10^{-15}	0.5000	10.6	0.200	2.532	6.103	0.834	1.093	0.331	1.291
3	0.015	10^{-19}	1.0000	42.2	0.188	2.532	10.60	0.936	1.099	0.527	1.045
4	0.032	10^{-16}	0.1250	12.6	0.398	2.535	5.638	0.838	1.095	0.189	1.376
5	0.046	10^{-12}	0.0625	5.31	0.398	2.528	5.623	0.841	1.091	0.181	1.358
6	0.048	10^{-02}	0.1250	2.82	0.224	2.535	6.482	0.956	1.095	0.458	1.093
7	0.054	10^{-01}	0.0625	4.47	0.141	2.527	14.40	1.021	1.195	0.402	1.262
8	0.063	10^{-11}	0.2500	5.01	0.266	2.522	5.683	0.842	1.089	0.246	1.315
9	0.063	10^{-17}	1.0000	20.0	0.112	2.521	7.534	0.823	1.089	0.434	1.186
10	0.064	10^{-19}	1.0000	42.2	0.178	2.528	10.65	0.942	1.098	0.537	1.135
11	0.069	10^{-01}	0.1250	2.11	0.282	2.539	5.821	0.950	1.097	0.188	1.379
12	0.077	10^{-16}	0.5000	13.3	0.224	2.521	6.273	0.832	1.088	0.361	1.282

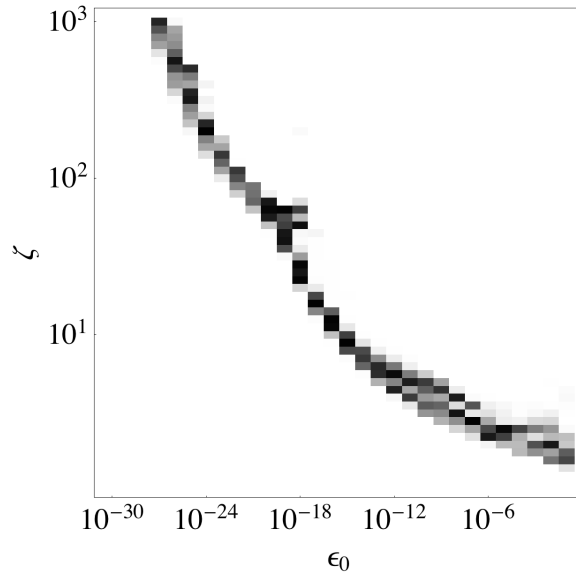


Fig. 3: Projection of $\exp(-\chi^2/3)$ on the (ε_0, ζ) plane, while the value of Δ is adjusted to yield the minimum χ^2 at each grid site.

3.2. Parameter sets with small values of χ^2

More than 130 grid points are found to yield χ^2 less than 1. Among them, 12 cases have $\chi^2 < 0.1$, which are listed in Table 2 with the resulting abundances of light

Table 3: The parameter sets with minimum χ^2 for each value of ε_0 . Only the cases with $\chi^2 < 10$ are listed.

ε_0	Δ	ζ	T_{09} [10^9K]	χ^2	D/H [10^{-5}]	T/H [10^{-8}]	$^3\text{He}/\text{H}$ [10^{-5}]	$^6\text{Li}/\text{H}$ [10^{-14}]	$^7\text{Li}/\text{H}$ [10^{-10}]	$^7\text{Be}/\text{H}$ [10^{-10}]
10^{-20}	1	75.0	0.100	6.716	2.633	19.79	1.419	1.274	1.416	0.267
10^{-19}	1	42.2	0.188	0.015	2.532	10.60	0.936	1.099	0.527	1.045
10^{-18}	1/2	25.1	0.316	0.100	2.532	6.373	0.815	1.094	0.350	1.158
10^{-17}	1	20.0	0.112	0.063	2.521	7.534	0.823	1.089	0.434	1.186
10^{-16}	1/8	12.6	0.398	0.032	2.535	5.638	0.838	1.095	0.189	1.376
10^{-15}	1/2	10.6	0.200	0.011	2.532	6.103	0.834	1.093	0.331	1.291
10^{-14}	1/16	7.94	0.398	0.153	2.519	5.596	0.833	1.088	0.182	1.336
10^{-13}	1/16	6.31	0.398	0.235	2.539	5.669	0.861	1.096	0.189	1.537
10^{-12}	1/4	5.62	0.282	0.006	2.528	5.692	0.844	1.091	0.242	1.355
10^{-11}	1/4	5.01	0.266	0.063	2.522	5.683	0.842	1.089	0.246	1.315
10^{-10}	1/2	5.96	0.100	0.142	2.519	5.995	0.845	1.088	0.335	1.341
10^{-09}	1/8	3.55	0.355	0.148	2.536	5.657	0.852	1.095	0.190	1.305
10^{-08}	1/8	3.16	0.355	0.317	2.546	5.685	0.859	1.100	0.186	1.299
10^{-07}	1/8	2.99	0.335	0.151	2.545	5.711	0.880	1.099	0.200	1.376
10^{-06}	1/16	2.66	0.376	0.330	2.549	5.724	0.890	1.101	0.189	1.317
10^{-05}	1/16	2.99	0.299	1.351	2.538	5.947	0.939	1.096	0.412	1.532
10^{-04}	1/8	2.66	0.282	0.201	2.540	5.804	0.918	1.097	0.271	1.218
10^{-03}	1/4	2.82	0.178	0.345	2.535	5.774	0.887	1.096	0.248	1.181
10^{-02}	1/8	2.82	0.224	0.048	2.535	6.482	0.956	1.095	0.458	1.093
10^{-01}	1/16	4.47	0.141	0.054	2.527	14.40	1.021	1.195	0.402	1.262

elements. The number of minima itself is not meaningful since it will become larger if we take a finer mesh. In Table 3, the values of Δ , ζ and T_{09} which minimize χ^2 for each value of ε_0 considered here are presented together with the abundances of elements. There is no parameter set resulting in $\chi^2 < 10$ for $\varepsilon_0 \leq 10^{-21}$, and for $\varepsilon_0 \geq 10^{-19}$ the parameter sets with $\chi^2 < 1$ are found.

In all the cases listed, the proton and the ^4He abundances are found to be 0.753 and 0.247, respectively. The abundance of $^6\text{Li}/\text{H}$ is quite insensitive to the value of ε_0 , resulting in $^6\text{Li}/\text{H} \simeq 1.1 \times 10^{-14}$. The sum of abundances of ^7Li and ^7Be is constrained by the χ^2 calculation, and is consistent with the measured primordial lithium abundance for all the parameter sets with small χ^2 values listed in Table 2, while there are sizable variations in the abundances of ^7Li and ^7Be .

3.3. Evolution of abundances

The evolution of abundance of light elements is shown for two selected cases in Fig. 5 with (the solid lines) and without (the dotted lines) taking into account the NTD contributions. The left panels are for the set No. 1 in Table 2 with $\chi^2 = 0.006$,

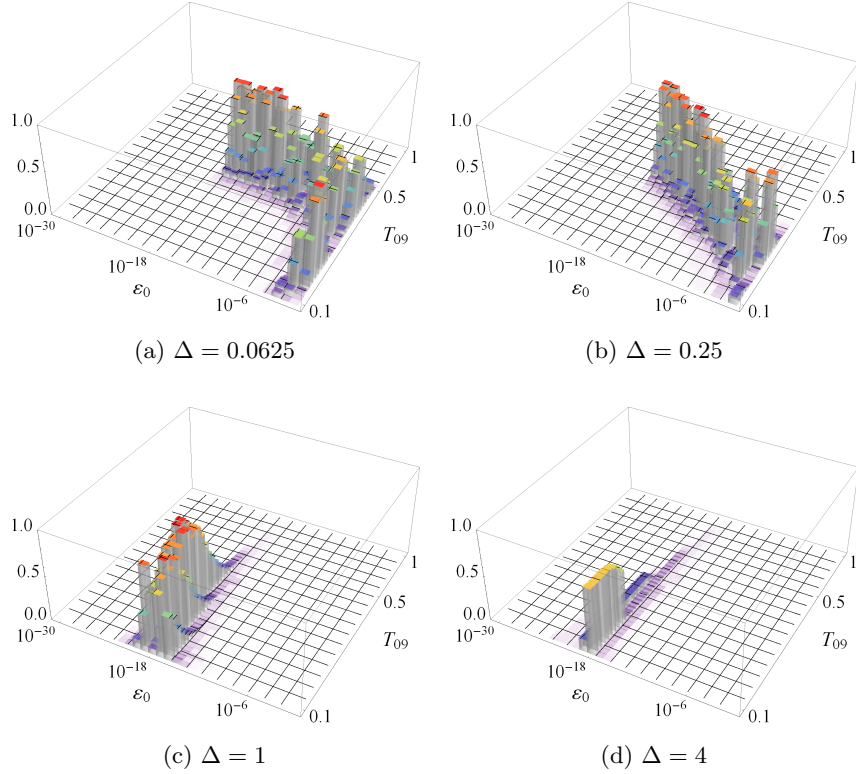


Fig. 4: The value of $\exp(-\chi^2/3)$ on the (ε_0, T_{09}) plane, where the width parameter is $\Delta = 0.0625$ (a), 0.25 (b), 1 (c) and 4 (d). The value of ζ is adjusted to yield the minimum χ^2 at each grid point.

and the right panels are for the set No. 4 with $\chi^2 = 0.032$. In the bottom panels, the relative ratios of the abundances with and without the NTD particles are plotted.

Several remarks are in order here. First, major changes occur during the period $0.5 \lesssim T_9 \lesssim 0.3$. Secondly, the NTD contribution is found to lower the abundances of ${}^3\text{He}$ and ${}^7\text{Be}$. The neutron, triton and ${}^7\text{Li}$ abundances increase during this period until $T_9 \simeq 0.35$ and then slightly decrease. ${}^7\text{Be}$ is dominant over ${}^7\text{Li}$, and the sum of the two is lowered by about one-third, as required by the observation. Thirdly, as the neutron abundance increases around $T_9 = (0.5 \sim 0.3)$ due to the NTD contribution, Coc et al.⁴⁰ have also concluded that the injection of extra neutrons at $T \simeq 50$ keV (or $T_9 \simeq 0.43$) can resolve the lithium problem but at the cost of over-predicting the deuterium abundance far beyond the observed values.

In Fig. 6, we show the changes in the production rate of light elements due to the NTD contribution

$$\Delta Y_i \equiv \frac{1}{H} \frac{d}{dt} [Y_i^{ntd} - Y_i^{th}], \quad (14)$$

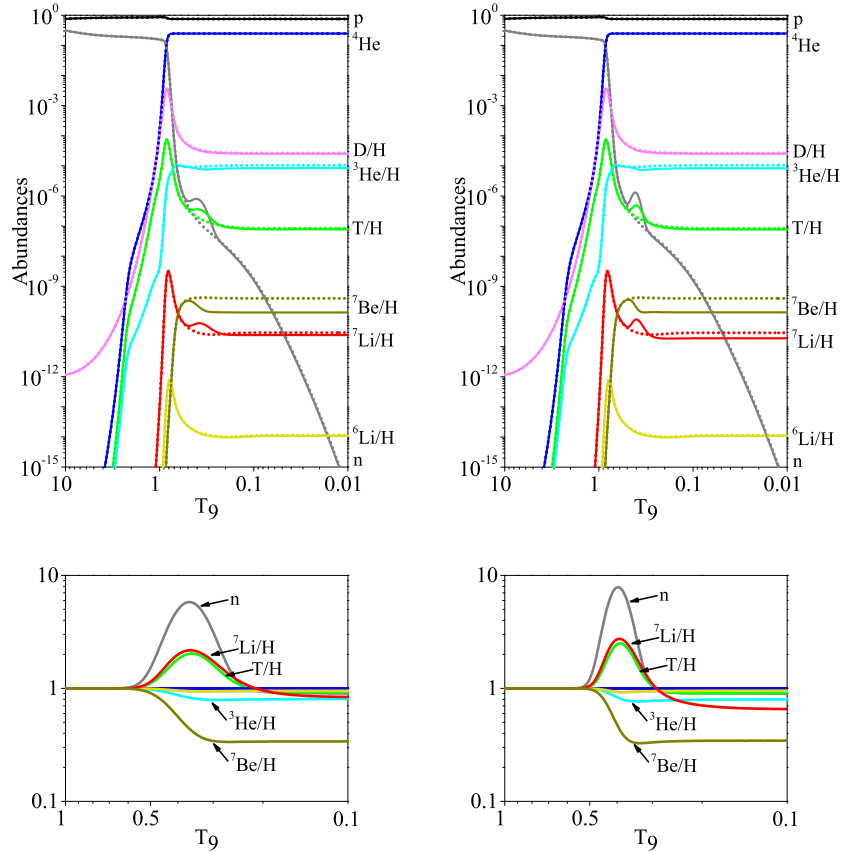
12 *Authors' Names*


Fig. 5: The abundances of elements with (the solid lines) and without (the dotted lines) the NTD effects are shown in the top panels, and the relative ratios of the abundances of elements with the NTD effects with respect to those without are plotted in the bottom panels. The left panels are for the parameter set No. 1 ($\varepsilon_0 = 10^{-12}$, $\Delta = 0.25$, $\zeta = 5.62$ and $T_0 = 0.282$), and the right panels are for the set No. 4 ($\varepsilon_0 = 10^{-16}$, $\Delta = 0.125$, $\zeta = 12.6$ and $T_0 = 0.398$) of Table 2.

where Y_i^{ntd} and Y_i^{th} denote the abundance of the neutron ($i = n$) as shown in Fig. 6(a) and that of the sum of ^7Be and ^7Li ($i = ^7\text{Be} + ^7\text{Li}$) as shown in Fig. 6(b) with and without the NTD contribution, respectively, and H is the Hubble parameter. The left and right panels are for the parameter sets No. 1 and No. 4 of Table 2, respectively. In addition to the net change (denoted by the solid lines), we have also plotted the contributions from a few important reactions, i. e., $p + n \rightarrow \text{D} + \gamma$, $\text{T} + \text{D} \rightarrow n + ^4\text{He}$, $^3\text{He} + n \rightarrow p + \text{T}$, $^7\text{Li} + p \rightarrow 2^4\text{He}$ and $^4\text{He} + \text{T} \rightarrow ^7\text{Li} + \gamma$. The general behaviors of the curves from both sets No. 1 and No. 4 are quite similar. We observe that the NTD component enhances the photo-disintegration of the

deuteron (the backward reaction of $p + n \rightarrow D + \gamma$) and $T + D \rightarrow n + {}^4\text{He}$ reaction, increasing the neutron abundance. On the other hand, ${}^3\text{He} + n \rightarrow p + T$ reaction is also enhanced by the NTD, and reduces the neutron abundance. The bottom panels of Fig. 5 also show the neutron abundance increases until $T_{09} \simeq 0.4$ as much as about 8 times of the SBBN value, and then decreases to the level of 0.9 times of the SBBN value.

The change in ${}^7\text{Li} + {}^7\text{Be}$ abundance is found to be dominated by the NTD contribution from the ${}^7\text{Li} + p \rightarrow 2{}^4\text{He}$ reaction. A high NTD temperature enhances the burning of ${}^7\text{Li}$ by allowing the proton to overcome the Coulomb barrier and to fuse with ${}^7\text{Li}$. Roughly a half of the reduction of Li due to this process is offset by the increase of ${}^7\text{Li}$ abundance through the ${}^4\text{He} + T \rightarrow {}^7\text{Li} + \gamma$ reaction. Due to the increased neutron abundance, the ${}^7\text{Be} + n \rightarrow p + {}^7\text{Li}$ reaction also increases the lithium abundance roughly as much as ${}^4\text{He} + T \rightarrow {}^7\text{Li} + \gamma$ reaction, but it lowers the same amount of ${}^7\text{Be}$ leaving the sum of ${}^7\text{Li} + {}^7\text{Be}$ unchanged. After summing the contributions from all the reactions, the lithium abundance is lowered to the measured value.

In Fig. 7, we plotted the abundances of the light elements as functions of the baryon-to-photon ration η . The solid lines are for the standard BBN without the NTD, and the dotted and dashed lines are for the parameter sets No. 1 and No. 4, respectively. It shows that the ${}^4\text{He}$ and D abundances are little changed, while the ${}^7\text{Li}$ abundance is substantially reduced, as required to resolve the ‘‘lithium problem’’. The abundance of ${}^3\text{He}/\text{H}$ is also found to be noticeably reduced by including the NTD. The parameter sets Nos. 1 and 4 give us ${}^3\text{He}/\text{H} = 0.85 \times 10^{-5}$,^a which is consistent with the upper limit evaluated in Ref.,⁴¹ ${}^3\text{He}/\text{H} \leq (1.1 \pm 0.2) \times 10^{-5}$. It is to be noted that the primordial abundance of ${}^3\text{He}$ is still uncertain, the only data available coming from the Solar system and solar-metallicity HII regions in the Galaxy.⁴¹ For this reason, we have not included the ${}^3\text{He}$ primordial abundance in our chi-square estimation; see Eq.(12).

4. Discussions

We have studied the consequences of introducing a small fraction of non-thermal particles during the BBN process, allowing its magnitude to be time-dependent so that it contributes only for a certain period. This work may be regarded as an extension of the work by Kang et al.²⁵ where the magnitude was treated as time-independent. This extension, however, widens enormously the parametric space to be explored. As the first step in this direction, we have made the assumption of Eq. (1). Therefore, the contributions from the NTD of particles have been modeled in such a way that the average reaction rates are a superposition of two Maxwellian reaction rates of temperature T and $T_{\text{NTD}} = \zeta T$ given by Eq. (1). The calculations are based on the Kawano code, and thus the advances in nuclear cross sections made

^a What is meant by ${}^3\text{He}/\text{H}$ here is the sum of ${}^3\text{He}/\text{H}$ and T/H in Table 2.

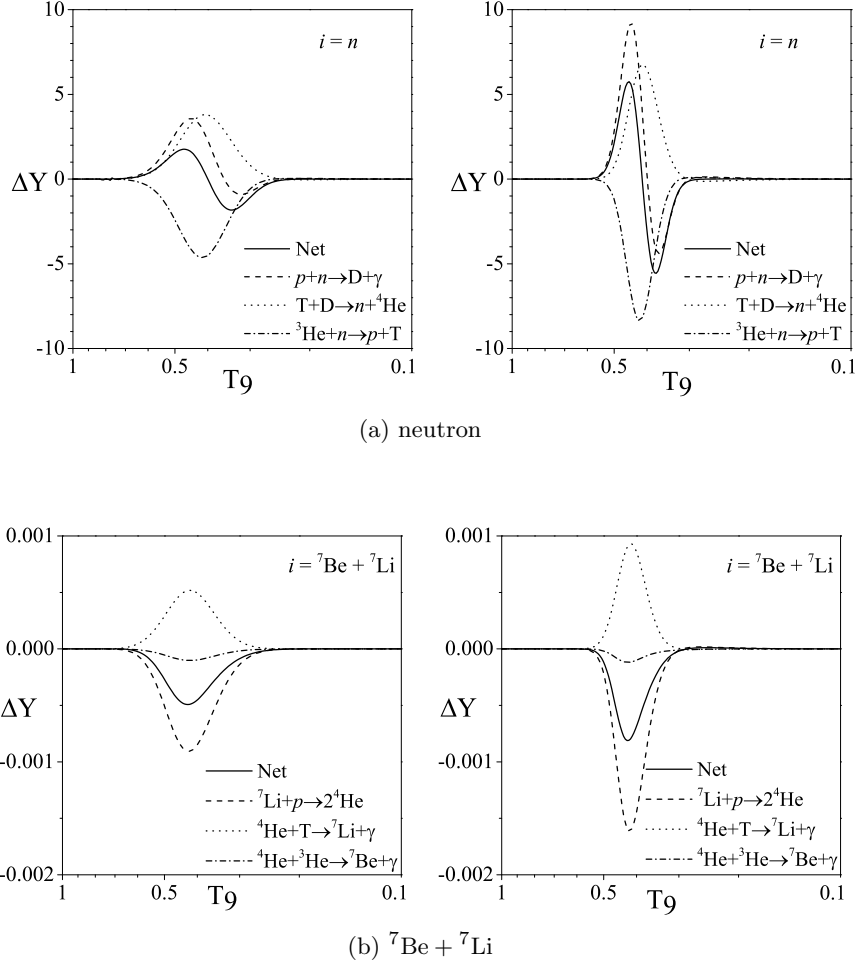
14 *Authors' Names*

Fig. 6: The NTD induced changes in the production rate, Eq. (14), for neutrons (top) and ${}^7\text{Be} + {}^7\text{Li}$ (bottom). The left and right panels are for the parameter set No. 1 and No. 4 of Table 2, respectively.

after the establishment of the Kawano code have not been taken into account.

With these caveats mentioned, we are in the position to discuss what is found. By scanning about half a million points in the parameter space, we have found more than 130 points which have χ^2 less than 1. Among them, twelve points have $\chi^2 < 0.1$, in good agreements with the observational data. Those minima are found to be scattered around in the parameter space.

When the width Δ is small, the parameters with small values of χ^2 turn out to be located in a narrow strip in the parametric space around $T_{09} \simeq 0.4$ and a

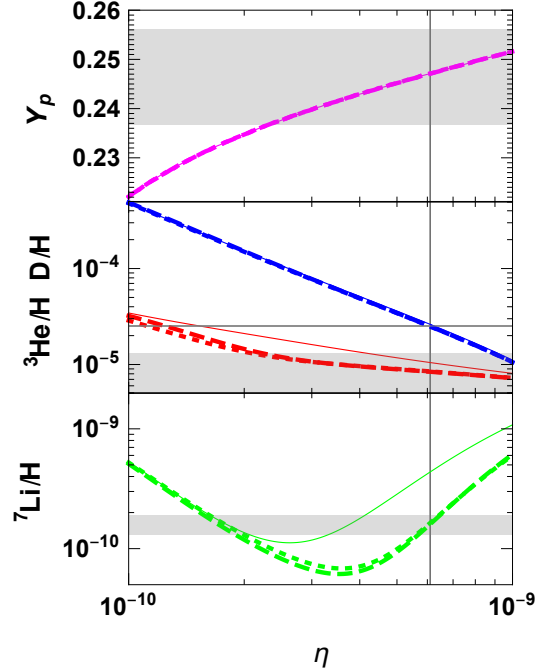


Fig. 7: The primordial abundances with respect to the baryon-to-photon ratio η . The solid lines are for the standard BBN, and the dotted and dashed lines are for the parameter set No. 1 and No. 4, respectively. The vertical line at $\eta = 6.10 \times 10^{-10}$ denotes the value of the ratio η obtained by the Planck,⁸ and the horizontal bands in gray are the observed light element abundances.³⁸

strong correlation between ε_0 and ζ is observed. When the width parameter is as small as 0.0625, the parameter sets with small χ^2 values exist over a range with $0.37 \lesssim T_{09} \lesssim 0.43$. The corresponding temporal range is $1300 \gtrsim t \gtrsim 950$ seconds. Our result is similar to the earlier study,²⁶ where it was discussed that the stau-NLSP and gravitino-LSP system with stau lifetime $\tau \simeq 10^3$ s could resolve the lithium problem with some representative values of the model parameters. If the width is as large as $\Delta = 1$, we could still find a large number of parameter sets with small χ^2 which, however, turns out to be scattered in rather a broad region in the T_{09} parametric space. This may imply that there can be diverse NTD-induced mechanisms that can bring the BBN predictions to the observation data. It is certainly necessary to refine the model to overcome the above mentioned limitations to identify the reaction channels responsible for the cure of the lithium problem.

It would be very useful and interesting to understand what happens when some of the underlying assumptions are released. Furthermore, we have not yet discussed

“chemical spectrum” of cosmic rays, which will enlarge the parametric space enormously. These extensions are under progress by making use of an updated version for the Kawano code.

Acknowledgements

We would like to thank Chung Yeol Ryu and Sang-In Bak for valuable discussions. This work was supported by the National Research Foundation of Korea (NRF) funded by the Ministry of Education, Science and Technology (2017R1A2B4012758 and 2013M7A1A1075764). TSP was also partly supported by the Institute for Basic Science (IBS-R031-D1).

References

1. R. A. Alpher and R. C. Herman, *Phys. Rev.* **74** (1948) 1737.
2. D. N. Schramm and R. V. Wagoner, *Annu. Rev. Nucl. Part. Sci.* **27** (1977) 37.
3. P. J. E. Peebles, D. N. Schramm, E. L. Turner and R. G. Kron, *Nature* **352** (1991) 769.
4. M. S. Smith, L. H. Kawano and R. A. Malaney, *Astrophys. J. Suppl.* **85** (1993) 219.
5. S. Sarkar, *Rep. Prog. Phys.* **59** (1996) 1493.
6. G. Steigman, *Annu. Rev. Nucl. Part. Sci.* **57** (2007) 463.
7. D. N. Spergel *et al.*, *Astrophys. J. Suppl.* **148** (2003) 175.
8. P. A. R. Ade *et al.* (Planck Collaboration), *Astron. Astrophys.* **571** (2014) A16.
9. J. Melendez and I. Ramirez, *Astrophys. J. Lett.* **615** (2004) L33.
10. M. Asplund, D. L. Lambert, P. E. Nissen, F. Primas and V. V. Smith, *Astrophys. J.* **664** (2006) 229.
11. M. Kusakabe, T. Kajino and G. J. Mathews, *Phys. Rev.* **59** (2006) 023526.
12. R. H. Cyburt, B. D. Fields and K. A. Olive, *J. Cosmol. Astropart. Phys.* **11** (2008) 012.
13. F. Iocco, G. Mangano, G. Miele, O. Pisanti and P. D. Serpico, *Phys. Rep.* **472** (2009) 1.
14. B. D. Fields, *Annu. Rev. Nucl. Part. Sci.* **61** (2011) 47.
15. G. Israelian, *Nature* **489** (2012) 37.
16. L. Sbordone *et al.*, *Astron. Astrophys.* **522** (2010) A26.
17. A. J. Korn *et al.*, *Nature* **442** (2006) 657.
18. X. Fu, A. Bressan, P. Molaro and P. Marigo, *Mon. Not. R. Astron. Soc.* **452** (2015) 3256.
19. M. Spite, F. Spite and P. Bonifacio, *Mem. Soc. Astron. Ital. Suppl.* **22** (2012) 9.
20. F. Iocco, *Mem. Soc. Astron. Ital. Suppl.* **22** (2012) 19.
21. M. Tanabashi *et al.* (Particle Data Group), *Phys. Rev. D* **98** (2018) 030001.
22. V. T. Voronchev, Y. Nakao and M. Nakamura, *Astrophys. J.* **725** (2010) 242.
23. V. T. Voronchev, Y. Nakao, K. Tsukida and M. Nakamura, *Phys. Rev. D* **85** (2012) 067301.
24. C. A. Bertulani, J. Fuqua and M. S. Hussein, *Astrophys. J.* **767** (2013) 67.
25. M. M. Kang, Y. Hu, H. B. Hu and S. H. Zhu, *J. Cosmol. Astropart. Phys.* **05** (2012) 011.
26. S. Bailly, K. Jedamzik and G. Moultaqa, *Phys. Rev. D* **80** (2009) 063509.
27. K. Jedamzik and M. Pospelov, *New J. Phys.* **11** (2009) 105028.

Instructions for typing manuscripts (paper's title) 17

28. L. Kawano, *Let's Go: Early Universe. Guide to Primordial Nucleosynthesis Programming*, FERMILAB-PUB-88-34-A (1988).
29. L. Kawano, *Let's Go: Early Universe. 2. Primordial nucleosynthesis: The computer way*, FERMILAB-PUB-92-004-A (1992).
30. R. V. Wagoner, W. A. Fowler and F. Hoyle, *Astrophys. J.* **148** (1967) 3.
31. R. V. Wagoner, *Astrophys. J. Suppl.* **18** (1969) 247.
32. R. V. Wagoner, *Astrophys. J.* **179** (1973) 343.
33. W. A. Fowler, G. R. Caughlan and B. A. Zimmerman, *Annu. Rev. Astron. Astrophys.* **5** (1967) 525.
34. W. A. Fowler, G. R. Caughlan and B. A. Zimmerman, *Annu. Rev. Astron. Astrophys.* **13** (1975) 69.
35. M. J. Harris, W. A. Fowler, G. R. Caughlan and B. A. Zimmerman, *Annu. Rev. Astron. Astrophys.* **21** (1983) 165.
36. G. Beaudet and P. Goret, *Astron. Astrophys.* **49** (1976) 415.
37. J. Beringer *et al.* (Particle Data Group) *Phys. Rev. D* **86** (2012) 010001.
38. K. A. Olive *et al.* (Particle Data Group) *Chin. Phys. C* **38** (2014) 090001.
39. R.H. Cyburt, B.D. Fields, K.A. Olive, and T.-H. Yeh, *Rev. Mod. Phys.* **88** (2016) 015004.
40. A. Coc, M. Pospelov, J. P. Uzan and E. Vangioni, *Phys. Rev. D* **90** (2014) 085018.
41. T.M. Bania *et al.*, *Nat.* **415** (2002) 54.